Theor Chim Acta (1992) 84: 217–235

Theoretica Chimica Acta

Molecular structure of mono- and dicarbonyls of rhodium and palladium

I. Pápai[1,*], A. Goursot[2], A. St-Amant[1,], and D. R. Salahub[1]**

[1] Département de Chimie, Université de Montréal, C.P. 6128, Succursale A, Montréal, Québec, Canada H3C 3J7

[2] Laboratoire de Chimie Organique Physique, URA 418 CNRS, ENSCM, 8 rue de l'Ecole Normale, F-34053 Montpellier, France

Received September 20, 1991/Accepted April 1, 1992

Summary. Density Functional Theory has been applied to the study of the molecular structure of neutral and positively charged mono- and dicarbonyls of rhodium and palladium. The calculated optimized geometries, dissociation energies and normal frequencies are reported for the MCO, MCO^+, $M(CO)_2$ and $M(CO)_2^+$ systems (where M = Rh and Pd), and the trends are discussed in detail. For neutral carbonyls, we interpret the M–C bond strength in terms of σ repulsion, which must be avoided, and π attraction. These are related to the metal atom properties, such as the atomic splittings and the atomic ionization energies. In ionic carbonyls, the bonding is characterized by electrostatic attraction and σ repulsion. The rhodium carbonyls are generally found to be more stable than the corresponding palladium carbonyls. The palladium dicarbonyls are found to be linear, while both linear and bent structures are stable for rhodium dicarbonyls. An interpretation of these trends is made.

Key words: Rhodium – Palladium – Dicarbonyls of Rh/Pd – Monocarbonyls of Rh/Pd – Density functional theory

1 Introduction

Both palladium and rhodium, mostly in their supported form, are commonly used as catalysts in the chemical and petroleum industries. The applications cover a wide range of chemical reactions, such as the hydrogenation of fats, hydrocarbons, sugars etc., hydrocracking of petroleum hydrocarbons, and many others [1]. They are also used in the automotive industry for CO oxidation in the catalytic converters that control automobile exhausts. Despite the fact that Pd and Rh are neighbours in the periodic table, they show quite different behaviour in some catalytic reactions, for example, CO hydrogenation [2].

* *Permanent address:* Institute of Isotopes of the Hungarian Academy of Sciences, H-1525 Budapest, P.O.B. 77, Hungary

** *Present address:* School of Pharmacy, University of California at San Francisco, San Francisco, California 94143, USA

Transition metal complexes are very often used as simple models to understand the nature of the metal-ligand bonding in catalytic processes. Several experimental techniques have been applied to investigate the bonding in transition metal complexes. Gas phase experiments [3] and matrix isolation spectroscopy [4] made a substantial contribution to the chemistry of transition metal-ligand interaction. On the other hand, accurate theoretical calculations offer an alternative source of information. Computational methods based on Density Functional Theory (DFT) [5, 6], at the Local Density level or, better with non-local, density gradient corrections, are among the most promising quantum chemical techniques in transition metal chemistry.

The transition metal-carbonyl interaction is of special interest for catalytic and organometallic systems [7]. The bonding between a transition metal atom and one or more CO ligands has been the object of a large number of theoretical studies (for recent publications see for example Ref. [8–13, 58]. The classical Dewar–Chatt–Duncanson model [14, 15] of the M–CO bond involves charge donation from CO to the metal in the σ space, and π back-donation from the metal d_π orbitals to the empty $2\pi^*$ orbital of CO. Bagus et al. [16] pointed out that it is also important to consider σ interactions with full (doubly occupied) metal nd_σ or $(n+1)s$ orbitals. These latter interactions, in contrast to the traditional attractive σ-donation, are repulsive (Pauli repulsion). The repulsion can be reduced by hybridization of the metal nd_σ and $(n+1)s$ orbitals with possible accompanying promotion between them, or metal charge polarization away from CO. This repulsion can also be avoided in the case of a cluster or of an infinite solid by transferring the electrons from the antibonding M-5σ orbital to lower lying vacant states in the metallic band. Since the 5σ orbital of CO has a small C–O antibonding character, the σ donation may slightly strengthen the C–O bond. The π interaction is attractive and, due to the charge transfer from the metal to the CO $2\pi^*$ orbital, the C–O bond is weakened, and therefore the C–O bond distance is lengthened, the C–O bond order is decreased and the ν_{CO} frequency shifts to lower wavenumbers with respect to the corresponding values in the free CO molecule. The M–CO bond strength is ultimately determined by both σ and π contributions. Thus the electron configuration of the atomic asymptotes of the metal (number of σ and π electrons) and the ionization potential of the metal atoms (as a measure of the ability for back-donation) are factors that can be related to the metal-carbonyl bond strength. On the other hand, the stability of the M–CO complex is connected with the promotion energy necessary to reach the atomic configuration in the molecule from its atomic asymptote. Therefore the separations of the low lying metal atomic states can be used to help rationalize the energetics of the metal carbonyls.

The nature of the bonding in the positively charged monocarbonyls has been extensively discussed by Barnes et al. [17]. The interaction of CO with a positive late transition metal ion is dominantly electrostatic, the importance of the π back-donation is reduced, while the metal d_σ-s hybridization and promotion play a prominent part in reducing the σ repulsion.

In the present paper we report a Linear Combination of Gaussian Type Orbitals – Model Core Potential – Density Functional (LCGTO-MCP-DF) study on the molecular structure of neutral and positively charged carbonyls of rhodium and palladium. The aim of our work is to contrast the calculated molecular properties of Rh and Pd carbonyls, and correlate them with the electronic structure of the two metal atoms.

2 Computational details

The LCGTO-MCP-DF formalism [18–20] and the analytical gradient expression for the LCGTO-MCP-DF energy [21] have been described in detail elsewhere. The program used in this study, called deMon [22, 23] employs a different approach to evaluate the energy gradient than that originally proposed [21]. Early tests [21, 24] indicated that large exchange-correlation fitting bases had to be used to obtain accurate forces. Subsequent work showed that more reliable forces were obtained when the exchange-correlation contribution to the energy gradient were integrated numerically. A larger set of grid points is used in this step since this numerical integration is more computationally demanding than the least squares fitting (LSF) procedure employed in the SCF process to fit the exchange-correlation contribution to the Fock matrix. So as to perform accurate numerical integrations, the weighting procedure proposed by Becke [25] was incorporated into deMon. In this paper, each calculation used a grid consisting of 32 spheres each containing 26 angular grid points in the LSF procedure and an augmented set of grid points consisting of the same 32 spheres with either 50, 110 or 194 angular grid points for evaluation of the gradients. For the latter procedure, the number of angular grid points in a given shell is increased when it is in a region where overlap from other atoms' grids might be important (this corresponds to radial shells at distances near the centre's Bragg–Slater radius).

For the Local Spin Density (LSD) calculations, the Vosko–Wilk–Nusair (VWN) [26] potential, considered to be "exact" within the Local Density Approximation (LDA), was chosen. For nonlocal calculations, Perdew and Wang's [27] correction to LSD exchange, and Perdew's [28] correction to LSD correlation were added to the VWN potential. It was found necessary to add a damping factor to the nonlocal exchange functional to avoid numerical instabilities in regions of very low density and relatively high gradient. This problem arises when nonlocal contributions are taken into account in the SCF procedure (Perdew's work did not include an SCF procedure). This is not a problem with the asymptotic form of the functional but simply numerical "noise" having to be controlled.

For Pd and Rh atoms an extended (Pd^{16+}, Rh^{15+}) model core potential has been used. The "semicore" 4*p* and the 5*s*, 5*p* and 4*d* valence orbitals have been treated explicitly. The scalar relativistic effects (mass velocity and Darwin terms) are incorporated into the model potentials [20]. The contraction pattern of the valence electron orbital basis sets for Pd and Rh are (2211/2111/121). For the carbon and oxygen atoms a triple-zeta plus polarization all electron basis set, with a (5211/411/1) contraction pattern was used. For hydrogen we used a (5*s*) orbital set contracted to [2*s*] augmented by a polarization function with exponent 0.5, yielding a (41/1) basis set. The auxiliary basis sets for the charge density (*CD*) and exchange-correlation potential (*XC*) fits were (3, 4; 3, 4) for Pd and Rh, (5, 2; 5, 2) for C and O, and (5, 1; 5, 1) for H. In the notation (k_1, k_2, l_1, l_2), k_1 (l_1) is the number of *s*-type gaussians in the *CD* (*XC*) basis and k_2 (l_2) is the number of *s*-, *p*- and *d*-type gaussians constrained to have the same exponent in the *CD* (*XC*) basis.

The equilibrium geometries were obtained at the local level (VWN potential) by gradient optimization. All bond distances and bond angles were simultaneously optimized, no symmetry constraint was imposed. Several initial geometries were tried so as to identify different minima on the potential energy surface. For a given dicarbonyl, we first determined the ground state at two

(linear and perpendicular) initial geometries, fixing the M–C and C–O bond lengths at the value we obtained for the corresponding monocarbonyl. Both structures were then optimized, yielding an energy minimum or a transition state, characterized by a vibrational analysis.

It has previously been shown that nonlocal corrections (NLC) to the exchange-correlation potential significantly improve binding energies [29, 30]. Therefore, we performed a self-consistent nonlocal calculation at the LDA equilibrium geometry of the molecules. All reported dissociation energies of carbonyls are computed at the nonlocal level with respect to the nonspherical (see in next section) ground state metal atoms (ions) and the optimized ground state ($^1\Sigma^+$) CO molecule. The zero point energy correction for the dissociation process of metal-carbonyls is small (less than 0.1 eV for monocarbonyls and less than 0.2 eV for dicarbonyls). The values are given in the appropriate tables.

The normal frequencies and normal coordinates were determined by diagonalizing the Hessian matrix built in the Cartesian representation. The elements of the Hessian were constructed by numerical differentiation of analytical gradients calculated about the equilibrium geometry using a displacement of $+0.02$ and -0.02 bohr for all $3N$ coordinates. Infrared intensities have been calculated for the neutral mono- and dicarbonyls using the double harmonic approximation [31]. Both vibrational frequencies and infrared intensities have been calculated at the LDA level.

3 Atoms and diatomics

The calculation of the energy difference between low lying states of transition metal atoms has always been a challenge for computational methods (see for example Refs. [32] and [33]). Only the most accurate *ab initio* methods are able to reproduce the experimental excitations within a few tenths of an electron volt. Nevertheless, this test is inevitable if one wishes to describe the molecular states accurately, since all the low lying atomic states of transition metals contribute more or less to the bonding. Although it is true that the lower symmetry of the molecule alleviates some of the problems related to atomic multiplet structure (for example, a closed-shell molecule may be "easier" than its open-shell atomic constituents) it, nevertheless, remains essential to have accurate atomic energies in order to determine dissociation energies.

In DF theory one is faced with a conceptual problem when treating open shell systems [34–36]. A given state (^{2S+1}L) of an open shell atom (or ion) is often described by a single configuration with $M_S = S$ with spherical averaging over M_L. In other words, a spherical charge density is enforced by use of fractional occupations, retaining the degeneracy of partially filled orbitals (d orbitals in the case of transition metal atoms). It has been shown [37] that removing the constraint of a spherical charge density lowers the atomic energies significantly if nonlocal functionals are used, in turn improving the binding energies of molecules. Therefore we have also determined the "nonspherical" atomic energies corresponding to different M_L, by use of integer occupations and breaking the degeneracy of partially filled orbitals. The lowest energy value has been used in the calculation of the dissociation energies. It must be remembered here, and in what follows, that both approaches, spherical or broken symmetry, correspond in general to an average over multiplets rather than to pure states, if the conventional wave function interpretation is made

Table 1. Atomic excitation energies (in eV) for Pd, Pd^+, Rh and Rh^+ calculated at local (LDA) and nonlocal (NLC) level using spherically averaged densities

Atom (ion)	El. conf.	State	LDA	NLC	Exp.[a]
Pd	s^0d^{10}	^1S	0.00	0.00	0.00
	s^1d^9	^3D	0.94	1.02	0.95
	s^2d^8	^3F	4.11	4.39	3.38
Pd^+	s^0d^9	^2D	0.00	0.00	0.00
	s^2d^8	^4F	3.71	3.95	3.19
E (ionization)[b]			9.18	9.20	8.51
Rh	s^1d^8	^4F	0.00	0.00	0.00
	s^0d^9	^2D	0.14	0.06	0.34
	s^2d^7	^4F	2.05	2.16	1.63
Rh^+	s^0d^8	^3F	0.00	0.00	0.00
	s^1d^7	^5F	2.28	2.42	2.13
E (ionization)[b]			8.15	8.12	7.48

[a] Experimental values are averaged over J states [67]

[b] The ionization energy is computed as a difference in total energy between the ground state atom and ion

(in exact Kohn–Sham DFT, an idealization, this would be taken care of by the functional).

The calculated atomic excitation energies for Pd, Pd^+, Rh and Rh^+, using the spherical approximation for the charge density, are listed in Table 1. Our LDA first excitation energies are within 0.2 eV of experiment (0.01 eV for ^3D-^1S for Pd, 0.20 eV for ^2D-^4F for Rh and 0.15 eV for ^5F-^3F for Rh^+) except for the ^4F-^2D splitting for Pd^+, where the difference is about 0.5 eV. Similar errors are observed for the second excitations of Pd (^3F-^1S) and Rh (^4F-^4F) atoms (0.7 and 0.4 eV respectively). These errors are consistent with the general feature of atomic LSD calculations: for a given atom the $d^{n-1}s^1$ configuration is overstabilized with respect to the $d^{n-2}s^2$ configuration (and similarly the d^ns^0 configuration is energetically favoured relative to $d^{n-1}s^1$) [32]. The NLC values are very similar to their LDA counterparts, typically within 0.2 eV and do not improve the results. We now point out the different nature of the Pd and Rh atomic separations. The Pd atom has a closed shell $4d^{10}5s^0$ (^1S) ground state, with the $4d^95s^1$ (^3D) first excited state, lying about 1.0 eV higher in energy. In the case of the Rh atom, the $4d^8s^1$ (^4F) state is the ground state lying just below the $4d^95s^0$ (^2D) first excited state. We will see in the next section that this ordering determines the stability of Pd and Rh carbonyls. The calculated ionization energies of the Pd and Rh atoms are slightly overestimated (by about 7–8%) at both levels of calculation, but the difference in the ionization potentials of Rh and Pd is very well reproduced: it is higher for Pd by about 1 eV. In summary, the errors introduced in the atomic separations and ionization potentials are relatively small and the trends are accurately reproduced in our calculations.

As further tests, equilibrium bond distances, vibrational frequencies and dissociation energies have been calculated for Pd and Rh hydrides and carbides. The spectroscopic constants obtained for the ground states of PdH, PdC, RhH

Table 2. LDA Spectroscopic constants of diatomic molecules (PdH, PdC, RhH and RhC)

Molecule	Method	State	R_e (Å)	ω_e (cm^{-1})	D_0 (eV)[a]	
PdH	this work	$^2\Sigma^+$	1.539	2173	2.59	(3.00, 2.59)
	MCPF[b]	$^2\Sigma^+$	1.540	1958	2.22	
	SOCI[c]	$^2\Sigma^+$	1.545	2081	2.34	
	exp.	$^2\Sigma^+$	1.534[d]	2036[e]	2.43 ± 0.26[f]	
PdC	this work	$^1\Sigma^+$	1.733	927	3.70	(4.91, 3.88)
	CI[g]	$^3\Sigma^-$	2.006	502	2.11	
	exp.	—	—	—	<4.46[h]	
RhH	this work	$^3\Delta$	1.553	2177	2.93	(3.68, 3.41)
	MCPF[b]	$^3\Delta$	1.575	2051	2.81	
	SOCI[c]	$^3\Delta$	1.576	1971	2.97	
	exp.	—	—	—	2.56 ± 0.22[f]	
RhC	this work	$^2\Sigma^+$	1.639	1124	6.27	(7.88, 6.93)
	CI[g]	$^2\Sigma^+$	1.714	821	2.92	
	exp.	$^2\Sigma^+$	1.614[i]	1050[i]	5.97[j]	

[a] Dissociation energies in the present work are calculated with respect to the nonspherical ground state atoms at the nonlocal level. Calculated values with respect to the spherical atoms at local and nonlocal level respectively are listed in parentheses. Zero point energy corrections included
[b] Modified Coupled Pair Functional results [48]
[c] Second Order Configuration Interaction results [45]
[d] Ref. [38].
[e] estimated from ν ($^{108}Pd^2D$) = 1446 cm^{-1} from Ref. [39]
[f] Ref. [42] [g] Ref. [49] [h] Ref. [41] [i] Ref. [41] [j] Ref. [44]

and RhC are summarized in Table 2 along with other theoretical results and available experimental data.

In general, experimental spectroscopic data for the second row transition metal heteronuclear diatomics are rather limited. From the molecules we have chosen, experimental bond distances and vibrational frequencies have been reported for PdH (more precisely for $^{108}Pd^2D$) [38, 39] and RhC [40, 41], and dissociation energies are known with varying accuracy for all four diatomics [42–44]. However, extensive and systematic *ab initio* studies, which can serve as a solid reference point for other methods, have been carried out for the second row transition metal hydrides by Balasubramanian [45–47] and Langhoff et al. [48]. Limited CI calculations have been published for PdC and RhC by Shim and Gingerich [49].

As one can see from Table 2, our R_e value for PdH is in remarkable agreement with both the experimental and other theoretical results. A vibrational frequency has been reported for $^{108}Pd^2D$ ($\omega_e = 1446\ cm^{-1}$). Based on this, one can estimate a value of $2035\ cm^{-1}$ for $^{106}Pd^1H$. Our calculated harmonic frequency is reasonably close to that value. The calculated dissociation energy is well within the experimental energy interval determined by ion beam measurements [42].

To our knowledge, PdC has not been observed experimentally in the gas phase. Only an upper limit of 4.46 eV has been estimated for its dissociation energy [43]. All electron HF and CI calculations are reported by the same authors [49], predicting the $^3\Sigma$ state to be the ground state. Quite different results

are found by the LCGTO-MCP-DF method. The ground state is determined to be $^1\Sigma$ and the R_e, ω_e values differ significantly. The rationalization of these discrepancies has previously been reported [50].

Contrary to PdH, no experimental bond distances and vibrational frequencies can be found in the literature for RhH. Theoretical studies indicate that $^3\Delta$ is the ground state. Our calculated R_e is about 0.02 Å shorter than the MCPF and SOCI results and the vibrational frequencies are reasonably close as well. All theoretical dissociation energies are slightly higher (by about 0.2–0.4 eV) when compared to experiment [42].

Detailed experimental information is available for RhC [40, 41], making it a suitable candidate for testing purposes. The LCGTO-MCP-DF bond distance is 0.025 Å shorter than the experimental value, and our ω_e falls rather close to the experimentally reported value. We note that limited CI calculations [49] (the same quality as for PdC) introduce significant errors for R_e and ω_e. Our calculated dissociation energy is very close to the experimental value.

In Table 2, we also list the LCGTO-MCP-DF dissociation energies with respect to the spherical atoms at the local and nonlocal levels (first and second numbers in parentheses). It is well known that LDA binding energies are usually too high, and our results for Pd and Rh diatomics are in accord with this general experience. In all cases nonlocal corrections improve (lower) the dissociation energies. Significant improvements are further made by removing the spherical density constraint. It is remarkable that for the Rh atom, the nonspherical total energy is lower by as much as 0.5 eV relative to the spherical total energy, illustrating the importance of using nonspherical atomic densities for accurate binding energies.

It is not the aim of the present work to analyse the electronic structure of Pd and Rh hydrides and carbides. Instead, we focus on the comparison of Pd and Rh molecules. Table 2 clearly shows that all the spectroscopic constants of PdH and RhH have comparable values. Also, their experimental dissociation energies are rather close. We obtained 1.07 for the M–H Mayer bond order [51] in both cases. In contrast, one can see significant differences in the spectroscopic constants of the carbides. For PdC the bond distance is longer by about 0.1 Å, the vibrational frequency is about 200 cm^{-1} lower, and the binding energy is smaller by about 2.3 eV compared to the corresponding values for RhC. The calculated M–C bond orders are 2.47 and 2.84 for PdC and RhC respectively, also indicating a stronger bond in RhC.

4 Monocarbonyls

Our results for PdCO, $PdCO^+$, RhCO and $RhCO^+$ are presented in Tables 3–6.

Although PdCO has been experimentally observed by infrared spectroscopy as a product of a co-condensation reaction of atomic Pd with CO in an argon matrix [52], there is no experimental data available for the geometry and the binding energy. However, among the second row transition metal monocarbonyls, PdCO is the most studied by different theoretical techniques [53–56, 58, 62]. A study by Pacchioni et al. [53] was the first to use a correlated technique, the multi-reference double-excitations configuration interaction (MRD CI) method using a nonrelativistic effective core potental (ECP), to investigate the electronic structure of PdCO. Later [54] they used the same method, but a different ECP to study the PdCO and RhCO molecules. Pacchioni

and Koutecky [55] have chosen PdCO as a model for the on top site chemisorbed CO on the Pd(111) surface. Rohlfing and Hay [56] have performed second order Møller–Plesset perturbation (MP2) [57] calculations to study the relative stability of mono- and tetracarbonyls of Ni, Pd and Pt using relativistic ECP (RECP). A systematic study on PdCO by Blomberg et al. [58] revealed that the relativistic corrections have a large effect on the binding energy and the equilibrium geometry. They applied different levels of theory, such as the complete active space SCF (CAS SCF) [59], the multi-reference contracted CI (MRC-CI) [60], and the modified coupled pair functional (MCPF) [61] method using all electron basis sets. Very recently, a GVB-PP (general valence bond with perfect singlet-pairing restrictions) [62] study has been presented by Smith and Carter for the interaction of CO (and NO) with Pd (and Pt) atoms.

The optimized geometries and dissociation energies of the ground state ($^1\Sigma^+$) of PdCO obtained by the above-mentioned methods are summarized in Table 3.

All methods find the ground state of PdCO to be the $^1\Sigma^+$ state, which correlates with the ground state ^1S Pd and $^1\Sigma^+$ CO asymptotes. The relatively large discrepancies in the calculated Pd–C distances and the dissociation energies demonstrates that even for relatively simple transition metal complexes, the agreement between the results obtained by different first principles methods is far from satisfying. Some general trends can clearly be found though. Because of the increased importance of π back-donation, the higher the degree of correlation incorporated into the calculations, the shorter the Pd–C equilibrium distance and the higher the binding energy. On the other hand, the inclusion of a relativistic correction always reduces the Pd–C equilibrium bond length and increases the binding energy.

Our LDA optimized Pd–C distance (1.814 Å) is shorter compared to values obtained by other methods. With the inclusion of nonlocal corrections, d_{Pd-C} is

Table 3. Optimized geometries (in Å) and dissociation energies (in eV) of the $^1\Sigma^+$ state of PdCO obtained by different methods

Method	d_{Pd-C}	d_{C-O}	D_e (eV)	Ref.
SCF	2.00 (2.18)[a]	1.159[b]	0.35 (0.0)[a]	[58]
CASSCF	1.90 (2.03)[a]	1.159[b]	0.87 (0.39)[a]	[58]
MRCCI12	1.87 (1.97)[a]	1.159[b]	1.21 (0.61)[a]	[58]
MCPF	1.86 (1.99)[a]	1.159[b]	1.47 (0.95)[a]	[58]
MRDCI20	2.11	1.159	0.31	[54]
MP2	1.882	1.185	1.62	[56]
GVB-PP	1.96	1.14	1.17	[62]
LDA/LDA[c]	1.814	1.157	3.08[f]	this work
NLC/LDA[d]	1.814	1.157	2.14 (2.08)[g]	this work
NLC/NLC[e]	1.917	1.166	2.16 (2.10)[g]	this work

[a] Results in parentheses refer to nonrelativistic calculations

[b] CO bond length fixed at the given value

[c] The geometry and D_e are calculated at the local level

[d] The geometry is optimized at local level, and nonlocal calculations are performed at the equilibrium geometry to obtain D_e

[e] The geometry is optimized at nonlocal level

[f] Zero point correction is 0.062 eV

[g] Values corrected for BSSE

lengthened by as much as 0.1 Å. The value of 1.917 Å is somewhere in the middle of the interval covered by results obtained by correlated methods including relativistic corrections. Since there is no experimental information, we view the precise geometry as an open question. LSD geometries are usually good to within two or three hundredths of an Ångstrom. Although it is possible that nonlocal corrections are as large as 0.1 Å, there is not yet a sufficient body of experience with self-consistent nonlocal corrections to conclude categorically (self-consistent calculations involve a gradient correction to the exchange-correlation potential and inaccuracies in handling divergencies of the potential and numerical instabilities may be a worry).

Despite the inclusion of nonlocal corrections, our dissociation energy is higher than any other value listed in Table 3. In order to rule out the basis set superposition error (BSSE) [63] as a source of the discrepancy, the BSSE was calculated at the nonlocal level at the (locally) optimized geometry of PdCO, and found to be insignificant (0.06 eV). We make a technical note here: the NLC/LDA (nonlocal corrections applied at the LDA geometry) and NLC/NLC dissociation energies in Table 3 differ only by 0.02 eV, showing that the error we introduce by calculating the binding energies at the locally optimized geometry is negligible.

We find a relatively large separation of the highest occupied and lowest unoccupied molecular orbitals (HOMO and LUMO) in the $^1\Sigma^+$ state of PdCO indicating that no close lying excited states are expected. The lowest lying triplet state ($^3\Sigma^+$) is about 2.9 eV higher in energy.

A band at 2050 cm^{-1} was assigned to the CO stretching mode of matrix isolated PdCO by Kündig et al. [52], which shows a shift of 88 cm^{-1} in ν_{CO} with respect to the band at 2138 cm^{-1} assigned to the monomeric CO in the matrix [52]. In their studies, the authors could not detect any $Pd(CO)_n$ ($n = 1-4$) modes in the far infrared region (500–200 cm^{-1}). They concluded that either the low frequency modes of $Pd(CO)_n$ are too weak to observe or they lie below 200 cm^{-1}. The calculated LDA harmonic CO stretching frequency in PdCO is 2099 cm^{-1} (Table 5), in good agreement with the observed value for the matrix isolated PdCO. We found a shift of 64 cm^{-1} in ν_{CO}, which is reasonably close to the shift observed in the matrix isolation experiments. The calculated infrared intensities corresponding to the ν_1 (CO str), ν_2 (PdC str) and ν_3 (PdCO bend) modes are 544, 4 and 8 km/mol respectively, showing that the low frequency modes (ν_2 and ν_3) are about two orders of magnitude weaker than ν_1. This can rationalize the difficulty of observing these modes in the far infrared spectra. To our knowledge, the only theoretical vibrational analysis performed on PdCO is by Smith and Carter [62]. They calculated 2253, 428 and 561 cm^{-1} for the ν_1, ν_2 and ν_3 modes by the GVB–PP method utilizing a 10 valence electron relativistic electron core potential for Pd. They predict 20 cm^{-1} for the shift in ν_{CO} due to the coordination.

Far fewer studies have been concentrated on the RhCO molecule. It has not been observed experimentally and there have been only a few theoretical investigations carried out [54, 64, 65].

The $^4\Delta$ and $^2\Sigma^+$ states of RhCO have been studied by Koutecky et al. [54], by the MRD CI method using a nonrelativistic ECP for Rh. They found that only the $^2\Sigma^+$ state is bound, by 0.17 eV, at its optimized geometry ($R_{RhC} = 2.05$ Å). The $^2\Delta$ state of RhCO, as a model for a carbonyl surface species on supported rhodium catalysts has been studied by McKee et al. [64]. Using a RECP for Rh, the geometry of RhCO was optimized at the Unrestricted Hartree–Fock (UHF) level and binding energies of 2.40 and 1.80 eV were obtained at the MP2 and MP3 levels. All electron and RECP HF studies have

Table 4. Optimized (NLC/LDA) geometries and binding energies of monocarbonyl molecules and ion

Molecule	State	Occupation	d_{M-C}	d_{C-O}[a]	D_e (eV)	ZP^b (eV)
PdCO	$^1\Sigma^+$	$\pi^4\delta^4\sigma^2$	1.814	1.157	2.14	0.062
$PdCO^+$	$^2\Sigma^+$	$\pi^4\delta^4\sigma^1$	1.868	1.135	2.04	0.068
RhCO	$^2\Sigma^+$	$\pi^4\delta^4\sigma^1$	1.758	1.169	2.66	0.073
$RhCO^+$	$^3\Delta$	$\pi^4\delta^3\sigma^1$	1.864	1.139	2.47	0.071

[a] Calculated equilibrium bond distance for free CO is 1.140 Å
[b] Zero point correction

been presented by Mains and White [65] for a number of small Rh molecules including the $^2\Sigma^+$ and $^4\Delta$ states of RhCO, but no correlation effects were included in their molecular calculations.

We find the $^2\Sigma^+$ state to be the ground state for RhCO, dissociating to Rh $5s^04d^9$ (^2D) and $^1\Sigma^+$ CO. Since the Rh d orbital is partially occupied, close lying doublet states are expected for RhCO. The $^2\Delta$ state, having a δ-hole, lies less than 0.1 eV above the $^2\Sigma^+$ state (at the optimized geometry of the ground state molecule). The optimized Rh–C and C–O bond lengths are 1.758 Å and 1.169 Å respectively, and the dissociation energy is found to be 2.66 eV with respect to the ground state Rh atom (^4F) (Table 4). The calculated harmonic frequencies are $\nu_1 = 2037$, $\nu_2 = 608$ and $\nu_3 = 348\ cm^{-1}$ with corresponding IR intensities of 532, 1 and 5 km/mol (Table 5).

Tables 4–6 reveal noticeable differences in the calculated molecular parameters of PdCO and RhCO. The equilibrium Pd–C distance is 0.056 Å longer than the Rh–C distance (Table 4), showing the opposite trend to what one would expect from the size of the 4d and 5s orbitals (because of the orbital contraction across the row, both 4d and 5s orbitals in Pd are less extended in space than in Rh). Also the MC stretching and MCO bending frequencies (Table 5) are both lower in PdCO, indicating a weaker M–C bond in PdCO. The M–C bond orders support this trend (Table 6), they are 1.32 and 1.71 for PdC and RhC. On the other hand, the optimized C–O bond length is longer in RhCO (by 0.012 Å), the CO stretching frequency is lower in RhCO (by about 60 cm^{-1}), and the C–O bond order has a smaller value in RhCO (2.20) than in PdCO (2.33). On the basis of all these findings, one can assume stronger π back-bonding in RhCO, which is not surprising, if we recall that the ionization potential of the Rh atom is 1 eV lower than that of the Pd atom. Charge donation is therefore

Table 5. Calculated (LDA/LDA) harmonic frequencies (in cm^{-1}) of MCO and MCO^+ (M = Pd and Rh). Infrared intensities (in km/mol) for the neutral molecules are shown in parentheses

Sym.	Assignment	PdCO[b]	$PdCO^+$	RhCO	$RhCO^+$
a_1	ν_1 CO str[a]	2099 (544)	2224	2037 (532)	2202
	ν_2 MC str	541 (4)	477	608 (1)	495
e	ν_3 MCO bend	261 (8)	283	348 (5)	304

[a] Calculated harmonic frequency for free CO is 2163 cm^{-1}
[b] Experimental CO stretching frequency in PdCO is 2050 cm^{-1} [52]

Table 6. Population analysis of monocarbonyls

Molecule	Bond order		Population		Atomic charges		
	Pd–C	C–O[a]	5*s*	4*d*	M	C	O
PdCO	1.32	2.33	0.75	9.11	+0.13	−0.06	−0.07
$PdCO^+$	1.02	2.56	0.35	8.80	+0.86	0.00	+0.14
RhCO	1.71	2.20	0.61	8.28	+0.11	0.00	−0.11
$RhCO^+$	1.17	2.52	0.48	7.65	+0.88	0.00	+0.12

[a] Bond order in free CO is 2.54

more preferred in the case of Rh. Also, the more diffuse Rh $d\pi$ orbitals should overlap more efficiently with CO π^*. The difference is even more enhanced for the ionization of the metal *d* electrons from their atomic asymptotes. The calculated ionization potentials for the Pd $4d^{10}5s^0\,(^1S) \rightarrow Pd^+4d^95s^0\,(^2D)$ and the Rh $4d^95s^0\,(^4F) \rightarrow Rh^+4d^85s^0\,(^5F)$ processes are 9.2 and 8.0 eV, showing a tendency in line with the experimental data. Moreover, the σ repulsion should be less important in RhCO, as deduced from the occupation of the metal σ orbitals in RhCO and PdCO, which are $4d^{0.95}5s^{0.61}$ and $4d^{1.59}5s^{0.75}$ respectively. The σ repulsion is reduced by the hybridization of metal $4d_\sigma$ and 5*s* orbitals. As was emphasized by Bauschlicher and Langhoff [66], one of the linear combinations of $4d_\sigma$ and 5*s* orbitals reduces the charge density along the molecular axis decreasing the repulsion in the σ space. This type of orbital is shown in Fig. 1a which may be compared with the figures of Ref. [66]. This combination is doubly and singly occupied in PdCO and RhCO, respectively. The other combination (Fig. 1b) gives a hybrid orbital having an increased charge density along the M–CO axis, but it is unoccupied in both monocarbonyls. The polarization of the metal sd_σ hybrid orbital (away from the CO molecule) is also visible in Fig. 1b. As a consequence of the hybridization, electron promotion is induced from the metal

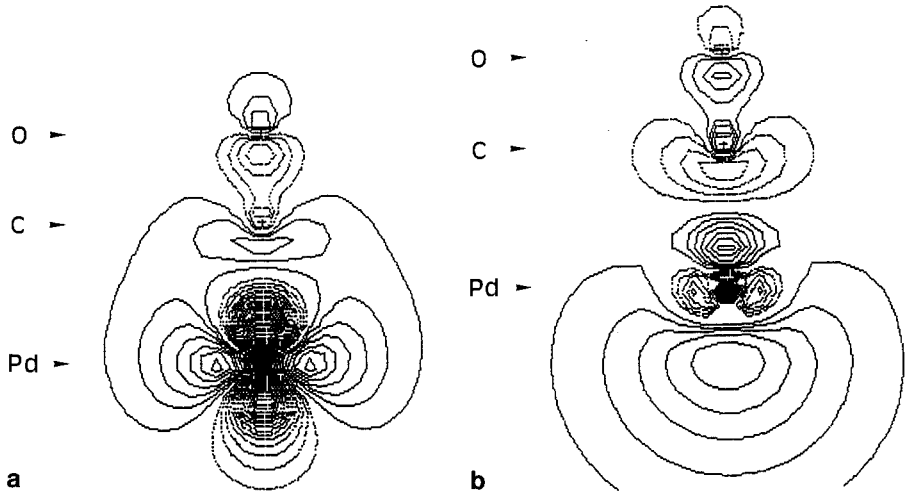

Fig. 1. Contour plots of the $4d_\sigma$-5*s* hybrid orbitals in $^1\Sigma^+$ PdCO. **a** highest occupied molecular orbital. **b** lowest unoccupied molecular orbital

$4d_\sigma$ to $5s$ orbitals. Both $^1\Sigma^+$ PdCO and $^2\Sigma^+$ RhCO have $4d^n5s^0$ metal atomic asymptotes. As it is shown in Table 6, the $4d \rightarrow 5s$ promotion is considerable in both cases, the electron configuration of the metal atom is $4d^{9.11}5s^{0.75}$ for Pd and $4d^{8.28}5s^{0.61}$ for Rh. However, the Pd $4d^{10}5s^0 \rightarrow 4d^95s^1$ promotion is energetically less favoured than the Rh $4d^95s^0 \rightarrow 4d^85s^1$ process, as we saw in the previous section. The former requires about 1 eV promotion energy, while the latter is an exothermic process. This rationalizes the difference in the stability of RhCO and PdCO (the calculated dissociation energies are 2.66 and 2.14 eV respectively). We note that our results are inconsistent with those of Koutecky et al. [54], who found significantly lower binding energies (0.17 and 0.31 eV for RhCO and PdCO), and predicted RhCO to be less stable.

We now consider the results we obtained for the monocarbonyl positive ions of Pd and Rh, summarized in Tables 4–6. The ground states are determined to be the $^2\Sigma^+$ and $^3\Delta$ states for $PdCO^+$ and $RhCO^+$. Both are derived from the $4d^n5s^0$ metal ion ground state ($4d^95s^0$ (^2D) for Pd^+ and $4d^85s^0$ (^3F) for Rh^+). This is in agreement with the results of Barnes et al. [17], who found the same ground states. The excited states have not been investigated in the present study.

Comparing the calculated molecular properties of the MCO^+ ions with their corresponding neutral molecules, the equilibrium M–C bond lengths (Table 4) are longer in the ions (by 0.054 and 0.106 Å), the MC stretching frequencies (Table 5) are shifted to lower values (by about 60 and 110 cm^{-1}), and the M–C bond orders (Table 6) are reduced (from 1.32 to 1.02 and from 1.71 to 1.17) in $PdCO^+$ and $RhCO^+$ respectively, relative to those of neutral molecules. This suggests weaker M–C bonds in the ionized monocarbonyls, which is mostly a consequence of the reduced $M \rightarrow CO$ π back-donation. The positive charge is mostly localized on the metal atom (Table 6) and therefore the CO molecule is polarized towards the metal ion, assuring the electrostatic attraction. The population analysis (Table 6) shows a $4d_\sigma$-$5s$ hybridization, although the $4d_\sigma \rightarrow 5s$ promotion is to a lesser degree than it is in the neutral molecules (the configuration of the metal ions in $PdCO^+$ and $RhCO^+$ are $4d^{8.80}5s^{0.35}$ and $4d^{7.65}5s^{0.48}$). Since the $4d^n5s^0$-$4d^{n-1}5s^1$ splitting is significantly larger for Pd^+ than for Rh^+ (1.4 eV is the calculated splitting, while experiment gives 1.1 eV), it is clearly expressed that $RhCO^+$ is relatively more stable than $PdCO^+$ (by 0.43 eV).

The equilibrium C–O distances in the MCO^+ ions are shorter than those in the MCO molecules, and even shorter than in the free CO molecule. Also the C–O bond orders have larger values in MCO^+ and they are very similar to the bond order in free CO (2.54). This follows from the reduced importance of the π back-donation and from the polarization effects (the CO in MCO^+ becomes similar to CO^+ which has a shorter bond length and larger bond order compared to neutral CO). Due to this, the CO stretching frequencies shift towards higher wavenumbers, 2224 and 2202 cm^{-1} for $PdCO^+$ and $RhCO^+$.

We calculated the adiabatic $MCO \rightarrow MCO^+$ ionization energies from the total energies of the ground state MCO and MCO^+ molecules. They are 9.1 and 8.3 eV for the Pd and Rh carbonyls, displaying the same trend as the atomic ionization potentials.

5 Dicarbonyls

The results obtained for $Pd(CO)_2$, $Pd(CO)_2^+$, $Rh(CO)_2$ and $RH(CO)_2^+$ are summarized in Tables 7–9.

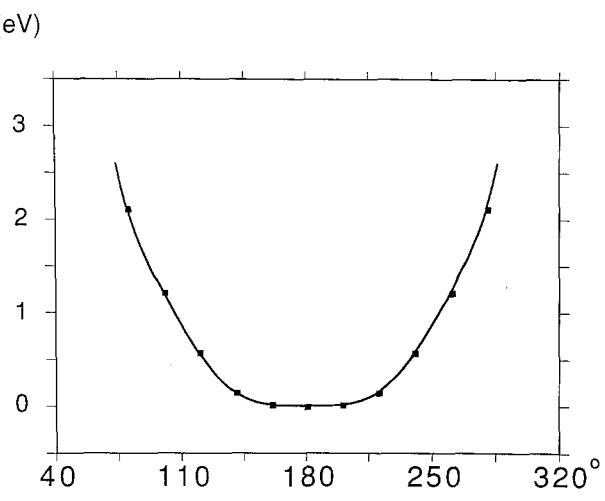

Fig. 2. C–Pd–C bending potential energy curve for $Pd(CO)_2$ obtained at the nonlocal level. The Pd–C and C–O bond distances were fixed at 1.908 Å and 1.149 Å respectively

We found two stationary points for the ground state of $Pd(CO)_2$ at the local level. The linear structure ($^1\Sigma^+$) has a negative CPdC bending mode, indicating that it is a transition state. A C_{2v} minimum was found at $\beta_{CPdC} = 151°$ and $\alpha_{PdCO} = 170°$; however, it is only less than 0.01 eV lower in energy relative to the transition state. The extremely flat bending potential is also apparent from the low value of the CPdC bending frequency of the bent structure, which is 40 cm^{-1} (Table 8). The C_{2v} geometry is not favoured anymore according to the nonlocal binding energies. The energy difference becomes 0.09 eV favouring the linear $Pd(CO)_2$. In order to check if there is any C_{2v} minimum at the nonlocal level, we derived a potential energy curve varying only the CPdC bending angle. Figure 2 shows a monotonic increase in total energy from the linear geometry, excluding a stable C_{2v} molecule. In accord with the local results, the bending potential is very flat around $\beta_{CPdC} = 180°$. The predicted linear structure is in agreement with the matrix isolation IR results of Kündig et al. [52], who assigned a band at 2044 cm^{-1} to the linear $Pd(CO)_2$ molecule. The calculated harmonic frequency for the asymmetric CO stretching mode ($\nu_6 = 2086$ cm^{-1} in Table 8), is slightly smaller than the calculated ν_{CO} in PdCO ($\nu_1 = 2099$ cm^{-1} in Table 5), showing the same trend as the experiment (Kündig et al. report 2050 and 2044 cm^{-1} for PdCO and $Pd(CO)_2$ respectively). It should be noted that our vibrational analysis presented in Table 8 was performed for the bent minima, but due to the flat bending potential, the CO stretching frequencies are not expected to vary as the CPdC angle changes from 151° to 180°. Indeed, for the linear transition state we find ν_6 to be 2095 cm^{-1}.

Comparing the calculated molecular parameters of $Pd(CO)_2$ with those of PdCO, we find that the Pd–C bond is weaker in the dicarbonyl: d_{PdC} is lengthened (by about 0.1 Å), the metal-carbonyl frequencies shift to lower wavenumbers, and the Pd–C bond order decreases (from 1.3 to 0.9) as the second CO binds. Although the bonding in $Pd(CO)_2$ and PdCO is similar in the sense that it is characterized by the σ repulsion and the π attraction, the balance between these two mechanisms is different. The Pauli repulsion is still reduced by the $5s$-$4d_\sigma$ hybridization, but the $4d_\pi$ Pd $\rightarrow 2\pi^*$ CO back-donation per CO molecule is smaller in $Pd(CO)_2$ than in PdCO, yielding a weaker Pd–C bond. The reduced π back-donation in $Pd(CO)_2$, which is also visible from the C–O

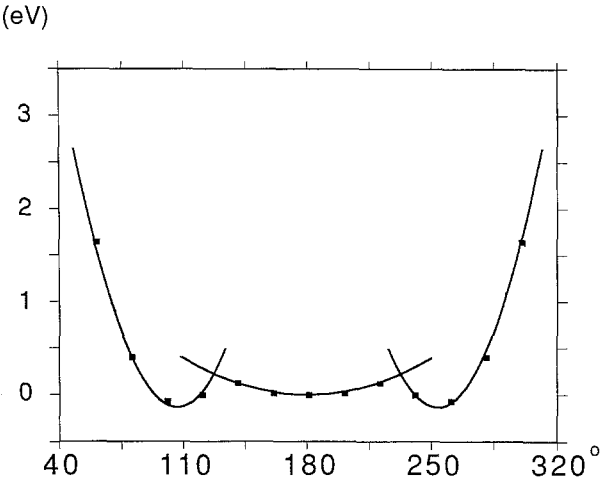

Fig. 3. C–Rh–C bending potential energy curve for $Rh(CO)_2$ obtained at the nonlocal level. The Rh–C and C–O bond distances were fixed at 1.832 Å and 1.161 Å respectively

bond lengths and C–O bond orders in PdCO and $Pd(CO)_2$ (Tables 6 and 9), has an impact on the energetics of the $Pd(CO)_2 \rightarrow PdCO + CO$ dissociation. The binding energy of the second CO is reduced compared to the dissociation energy of PdCO, we find 2.14 and 1.73 eV for the first and second CO, respectively.

Contrary to $Pd(CO)_2$, we found two minima ($D_{\infty h}$ and C_{2v}) for $Rh(CO)_2$. Despite a large difference in geometries, (the two carbonyls are close to perpendicular in the bent structure), they have very similar energies. At the local level, the bent molecule is more stable (by about 0.2 eV), while the NLC calculations indicate that the linear molecule is preferred (by about 0.1 eV). Figure 3 shows the bending potential of $Rh(CO)_2$ we obtained at the nonlocal level, which is rather different from that of $Pd(CO)_2$ (Fig. 2). It should be noted that to generate Fig. 3 the Rh–C and C–O bond distances were kept fixed at their optimized C_{2v} values and hence, the C_{2v} minimum is artificially too low, relative to the linear one, and therefore the bent structure appears to be more stable in Fig. 3. Nevertheless, we are dealing with relatively small energy differences (a few tenths of an eV), and we can definitely say, no matter what level of calculation we use, that both structures have about the same stability. Moreover, the energy barrier between the two structures are of the same order, i.e. a few tenths of an eV.

Why do we get two minima for $Rh(CO)_2$ and only one for $Pd(CO)_2$? We would like to answer this question remaining within the σ repulsion–π attraction picture and using MO terminology. First of all, it is worth noting that in linear dicarbonyls, for symmetry reasons, the negative combination of the two 5σ CO orbitals (labelled $5\sigma^-$ on Fig. 4) does not interact with the metal σ orbitals of s or d character. As depicted in a simplified way in Fig. 4, the only metal orbital which can mix with $5\sigma^-$ CO is p_z. However, this interaction is very weak in both $Pd(CO)_2$ and $Rh(CO)_2$, since the metal p orbitals are unoccupied. Breaking the $D_{\infty h}$ symmetry of the $M(CO)_2$ molecule, the nature of the σ repulsion is changed. In addition to the $5\sigma^+$ CO-metal repulsion, some of the metal d orbitals become repulsive to the $5\sigma^-$ CO combination. In Fig. 4, we see that for instance, for the rectangular $M(CO)_2$, (being positioned in the yz plane), the metal d_{yz} orbital is "σ-like" for both M–CO units. The $5\sigma^+$ CO-metal repulsion is reduced by the metal sd hybridization, (in our particular case, the

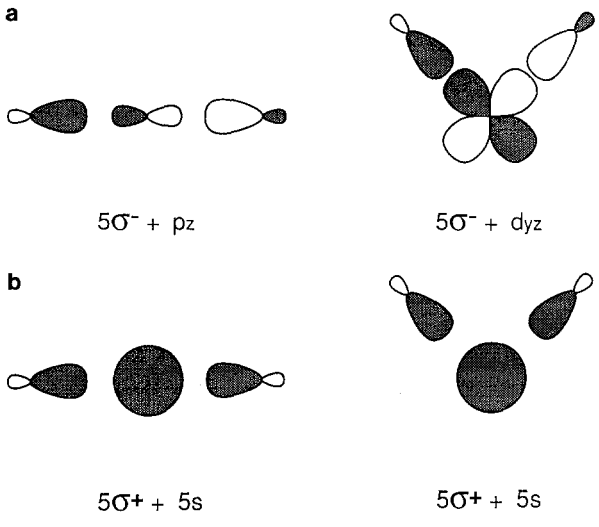

Fig. 4. Interaction of **a** $5\sigma^-$ CO and **b** $5\sigma^+$ CO orbitals with the metal orbitals in the linear and rectangular $M(CO)_2$ molecule

$5s$-$4d_{xx}$ hybridization), while the metal dp hybridization reduces the $5\sigma^-$ CO-metal repulsion, ($4d_{yz}$-$5p_y$, $5p_z$ hybridization in our coordinate system). The latter is energetically unfavourable for both $Pd(CO)_2$ and $Rh(CO)_2$, as the $4d \rightarrow 5p$ promotion requires much energy. As a consequence of this interaction, a metal-carbon antibonding orbital evolves in the region of metal d orbitals for both $Pd(CO)_2$ and $Rh(CO)_2$, and becomes more and more destabilized, as the bending angle decreases. Starting from the linear structure, the occupancy of this antibonding orbital switches from 2 to 1 in $Rh(CO)_2$ at about $\beta_{CRhC} = 130°$ (crossing of the $^2A_1$ and $^2B_2$ curves in Fig. 3), forming the $^2B_2$ state and giving rise to the C_{2v} minimum. The corresponding state, and therefore the C_{2v} minimum, cannot be formed in $Pd(CO)_2$, since all the metal originated orbitals are doubly occupied, yielding the answer to our question.

We note that the amount of metal $4d \rightarrow 2\pi^*$ CO charge transfer in the $M(CO)_2$ molecules, as deduced from the population analysis, hardly varies with respect to the bending angle, indicating that the attractive π interaction is not sensitive to the bending. Despite this, the calculated equilibrium Rh–C bond lengths and the Rh–C bond orders in linear and bent $Rh(CO)_2$ are noticeably different, which is likely related to the different nature of the σ repulsion.

The calculated dissociation energies (Table 7) show that $Rh(CO)_2$ is more stable relative to $Pd(CO)_2$. However, the binding energy of the second CO molecule in $Rh(CO)_2$ (1.75 eV) becomes very similar to that in $Pd(CO)_2$ (1.64 eV). It would be interesting to step further in the $Pd(CO)_n$–$Rh(CO)_n$ comparison for $n = 3$ and 4, but this was not the goal of the present study. The reduced π back-donation (per CO molecule) in $Rh(CO)_2$ (as compared to RhCO) is apparent from the calculated properties, just as we saw and discussed for $Pd(CO)_2$.

To our knowledge, no matrix isolation IR studies have been reported for the $Rh(CO)_n$ molecules. According to our results, the vibrational spectra are expected to be more complicated than the $Pd(CO)_n$ molecules, since both (linear and bent) structures of $Rh(CO)_2$ should be observed. The calculated harmonic frequencies and the IR intensities for the bent geometry of $Rh(CO)_2$ are listed in Table 8.

Table 7. Optimized geometries and binding energies (NLC/LDA) of dicarbonyl molecules and ions

Molecule	Sym.	State	d_{M-C}	d_{C-O}	α_{MCO}	β_{CMC}	D_e (eV)	ZP
$Pd(CO)_2$	C_{2v}	$^1A_1$	1.902	1.149	170.1	151.0	3.78[a] (1.64)[b]	0.12[c]
	$D_{\infty h}$	$^1\Sigma^+$	1.912	1.146	180.0	180.0	3.87 (1.73)	—
$Pd(CO)_2^+$	$D_{\infty h}$	$^2\Sigma^+$	1.961	1.131	180.0	180.0	3.87 (1.83)	0.18
	C_{2v}	$^2B_2$	1.934	1.135	169.8	99.4	3.36 (1.32)	—
$Rh(CO)_2$	C_{2v}	$^2B_2$	1.832	1.161	167.5	99.7	4.41 (1.75)	0.15
	$D_{\infty h}$	$^2\Sigma^+$	1.902	1.152	180.0	180.0	4.49 (1.83)	—
$Rh(CO)_2^+$	C_{2v}	$^1A_1$	1.818	1.141	177.1	85.9	4.30 (1.83)	0.18
	$D_{\infty h}$	$^3\Delta$	1.973	1.133	180.0	180.0	4.21 (1.74)	—

[a] ΔE ($M(CO)_2 \rightarrow M + 2CO$)
[b] ΔE ($M(CO)_2 \rightarrow MCO + CO$)
[c] Zero point correction

We identified two minima for the $Pd(CO)_2^+$ ion. As seen in Table 7, the linear structure is lower in energy by about 0.5 eV (by about 0.3 eV at the local level). The appearance of the C_{2v} minimum ($^2B_2$ state) is explained by the ionization from the destabilized Pd–C antibonding orbital. Similarly to $Rh(CO)_2$, this orbital is singly occupied in $Pd(CO)_2^+$. Looking at the calculated equilibrium Pd–C bond lengths and the Pd–C bond orders in linear and bent $Pd(CO)_2^+$, we have an example, where the energetically more stable structure ($^2\Sigma^+$) has a weaker Pd–C bond: d_{PdC} is longer and the Pd–C bond order is smaller for the linear ion. One can interpret this by the different nature of the σ repulsion in the linear and bent structure.

Two minima have been found for the $Rh(CO)_2^+$ ion as well. The linear $^3\Delta$ state can be derived from the ionization of a metal δ electron in the linear $Rh(CO)_2$, while the $^1A_1$ state originates from the bent $Rh(CO)_2$. The calculated dissociation energies for the two structures are very similar (Table 8). The bent

Table 8. Calculated harmonic frequencies (in cm^{-1}) of $M(CO)_2$ and $M(CO)_2^+$ (M = Pd and Rh). Infrared intensities (in km/mol) for the neutral molecules are shown in parentheses

Sym. assignment[a]			$Pd(CO)_2$[b] $^1A_1$	$Pd(CO)_2^+$ $^2\Sigma^+$	$Rh(CO)_2$ $^2B_2$	$Rh(CO)_2^+$ $^1A_1$
a_1	ν_1	CO str	2156 (79)	2272	2074 (359)	2226
	ν_2	MC str	480 (1)	410	577 (0)	632
	ν_3	MCO bend	374 (3)	446	521 (1)	532
	ν_4	CMC bend	40 (1)	62	84 (1)	104
a_2	ν_5	oop bend	242 (0)	278	260 (0)	371
b_1	ν_6	CO str	2086 (1674)	2219	2013 (1092)	2159
	ν_7	MC str	471 (93)	380	509 (29)	518
	ν_8	MCO bend	256 (1)	278	276 (3)	351
b_2	ν_9	oop bend	296 (4)	446	332 (4)	365

[a] C_{2v} notation is used for the linear molecules as well
[b] Experimental asymmetric CO stretching frequency for $Pd(CO)_2$ is 2044 cm^{-1} [52]

Table 9. Population analysis of dicarbonyls

Molecule		Bond order		Population		Atomic charges		
		Pd–C	C–O[a]	5*s*	4*d*	M	C	O
$Pd(CO)_2$	$^1A_1$	0.88	2.39	0.99	8.84	+0.14	−0.06	−0.01
	$^1\Sigma^+$	0.85	2.38	1.08	8.92	0.00	0.00	0.00
$Pd(CO)_2^+$	$^2\Sigma^+$	0.62	2.59	0.64	8.68	+0.70	0.00	+0.15
	$^2B_2$	0.73	2.56	0.55	8.57	+0.88	−0.07	+0.13
$Rh(CO)_2$	$^2B_2$	1.29	2.28	0.75	7.88	+0.28	−0.07	−0.07
	$^2\Sigma^+$	1.02	2.53	0.76	8.10	+0.12	−0.04	−0.02
$Rh(CO)_2^+$	$^1A_1$	1.19	2.47	0.56	7.72	+0.75	+0.02	+0.11
	$^1\Sigma^+$	0.81	2.52	0.30	7.94	+0.76	−0.01	+0.13

[a] Bond order for free CO is 2.54

ion is slightly favoured, but the energy difference is less than 0.1 eV. However, there is a remarkable difference in the calculated equilibrium Rh–C distances, 0.15 Å shorter for the bent ion, even shorter than in the bent neutral $Rh(CO)_2$. The Rh–C bond orders show the same trend. They are 1.2 and 0.8 for the $^1A_1$ and ^3A states respectively. This is because the $^1A_1$ state is a result of the ionization from the destabilized Rh–C antibonding orbital in the bent $Rh(CO)_2$ molecule, therefore both (spin up and down) Rh–C antibonding orbitals become unoccupied, yielding shorter Rh–C bond distances.

Based on the population analysis, which is summarized in Table 9, we can conclude that the bonding in the $M(CO)_2^+$ ions is similar to that in MCO^+ ions. The main attractive component of the bonding is the electrostatic interaction, since the positive charge is mostly localized on the metal atom, polarizing both CO molecules. However, the electrostatic attraction is shared between two carbonyls, therefore the second CO is less bound. The reduced importance of the π back-donation in the dicarbonyl ions is apparent from the calculated C–O bond lengths (Table 7), from the C–O bond orders (Table 9) and also from the relatively large values of the CO stretching frequencies (Table 8).

Finally we note that our equilibrium distances in both MCO^+ and $M(CO)_2^+$ ions are systematically shorter by as much as 0.15–0.20 Å compared to the MCPF results of Barnes et al. [17]. There is also a considerable discrepancy in the dissociation energies obtained by us and Barnes et al. [17]. In contrast to our results, they do not find noticeable differences in the stability of rhodium and palladium carbonyl ions (neither for mono-, nor for dicarbonyls). The discrepancies in the dissociation energies range from 50 to 80%, the MCPF values being smaller in all cases.

6 Conclusions

LCGTO-MCP-DF calculations on the MCO, MCO^+, $M(CO)_2$ and $M(CO)_2^+$ molecules, where M = Rh and Pd, have been presented in this paper. Our conclusions can be summarized as follows.

Despite the single configurational Kohn–Sham description, accurate atomic excitation energies and ionization potentials have been obtained for Pd, Pd^+, Rh and Rh^+.

The calculated spectroscopic constants of Pd and Rh hydrides and carbides are in good agreement with the available experimental data. The nonlocal corrections are essential to obtain accurate dissociation energies. The removal of the constraint of spherical charge density for atoms significantly improves the dissociation energies.

The metal-carbonyl bond is stronger in RhCO as compared to PdCO, caused by stronger π back-donation and less σ repulsion in RhCO. PdCO is less stable, since the $4d \rightarrow 5s$ promotion is energetically less favoured than for RhCO.

$Pd(CO)_2$ is linear, while both linear and bent $Rh(CO)_2$ are stable. This follows from the different nature of the σ repulsion in linear and bent dicarbonyls. The π back-bonding is not sensitive to the CMC bending.

The π back-bonding turns out to be less important in ionic carbonyls, the electrostatic attraction and the σ repulsion are the main components of the bonding.

The second CO is less bound in both neutral and ionic dicarbonyls, since the π back-donation (for neutral molecules) and the electrostatic attraction (for ions) is shared between the two CO molecules.

Noticeable discrepancies have been found between our results and those of *ab initio* MCPF calculations. The LDA equilibrium bond lengths are shorter; the inclusion of nonlocal corrections increases them somewhat but the discrepancy persists. The NLC dissociation energies are systematically higher than the MCPF results. A definitive conclusion as to which method yields more reliable results must await experimental data.

Acknowledgements. We are grateful to NSERC-Canada, and to the France-Québec program for support of this work.

Computing resources from Cray Canada, from the Services Informatiques de l'Université de Montréal, from the Centre National Universitaire Sud de Calcul (Montpellier), and the Centre de calcul de l'EPF-Lausanne are gratefully acknowledged. A. St-Amant thanks NSERC for a 1967 Science Scholarship. D. R. Salahub is grateful to the Canada Council for the award of a Killam fellowship.

References

1. Srivastava RD (1988) in: Heterogeneous catalytic science. CRC Press, Boca Raton
2. Stevenson SA, Raupp GB, Dumesic JA, Tauster SJ, Baker RTK (1987) in: Stevenson SA, Dumesic JA, Baker RTK, Ruckenstein E (eds) Metal-support interactions in catalysis, sintering, and redispersion. Van Nostrand Reinhold, NY, Chap 6, p 55
3. Metal-ligand bonding energetics in organotransition metal compounds. Polyhedron Symposia-In-Print Number 6, Polyhedron 7:1405 (1988)
4. Andrews L, Moskovits M (eds) (1989) Chemistry and physics of matrix-isolated species. North-Holland, Amsterdam
5. Hohenberg P, Kohn W (1964) Phys Rev 136:B864
6. Kohn W, Sham LJ (1965) Phys Rev 140:A1133
7. Cotton FA, Wilkinson G (1988) Advanced inorganic chemistry. Wiley, NY
8. Weltner W, Van Zee RJ (1989) in: Salahub DR, Zerner MC (eds) The challenge of d and f electrons, ACS, Washington, Chap 15, p 211
9. Barnes LA, Rossi M, Bauschlicher CW (1991) J Chem Phys 94:2031
10. Barnes LA, Bauschlicher CW (1989) J Chem Phys 91:314
11. Bauschlicher CH, Barnes LA, Langhoff SR (1988) Chem Phys Lett 151:391
12. Blomberg M, Brandemark U, Johansson J, Siegbahn P, Wenneberg J (1988) J Chem Phys 88:4324
13. Ziegler T, Tschinke V, Ursenbach C (1987) J Am Chem Soc 109:4825

14. Dewar MJS (1951) Bull Soc Chem Fr 18C:79
15. Chatt J, Duncanson LA (1953) J Chem Soc 2939
16. Bagus PS, Nelin CJ, Bauschlicher CW (1983) Phys Rev B28:5423
17. Barnes LA, Rosi M, Bauschlicher CW (1990) J Chem Phys 93:609
18. Sambe H, Felton RH (1975) J Chem Phys 62:1122
19. Dunlap BI, Conolly JWD, Sabin JR (1979) J Chem Phys 71:3396
20. Andzelm J, Radzio E, Salahub DR (1985) J Chem Phys 83:4573
21. Fournier R, Andzelm J, Salahub DR (1989) J Chem Phys 90:6371
22. St-Amant A, Salahub DR (1990) Chem Phys Lett 169:387
23. St-Amant A (1991) PhD Thesis, Université de Montréal
24. Pápai I, St-Amant A, Ushio J, Salahub DR (1990) Int J Quant Chem S24:29
25. Becke AD (1988) J Chem Phys 88:2547
26. Vosko SH (1980) Wilk L, Nausair M, Can J Phys 58:1200
27. Perdew JP, Wang Yue (1986) Phys Rev B33:8800
28. Perdew JP (1986) Phys Rev B33:8822; (1986) erratum: 38:7406
29. Becke AD in Ref. [8], Chap 12, p 165
30. Mlynarski P, Salahub DR (1991) Phys Rev B43:1399
31. Herzberg G (1945) Infrared and Raman spectra of polyatomic molecules. Van Nostrand, NY
32. Salahub DR (1987) Adv Chem Phys 69:447
33. Raghavachari K, Trucks GW (1989) J Chem Phys 91:1061
34. Ziegler T, Rauk A, Baerends EJ (1977) Theoret Chim Acta 43:261
35. von Barth U (1979) Phys Rev A20:1693
36. Wood JH (1980) J Phys B Atom Molec Phys 13:1
37. Kutzler FW, Painter GS (1987) Phys Rev Lett 59:1285
38. Knight LB, Weltner W (1971) J Mol Spectr 40:317
39. Malmberg C, Scullman R, Nylen P (1969) Ark Phys 39:495
40. Kaving B, Scullman R (1969) J Mol Spectr 32:475
41. Huber KP, Herzberg G (1979) Molecular spectra and molecular structure. IV. Constants of Diatomic Molecules. Van Nostrand Reinhold, NY
42. Tolbert MA, Beauchamp JL (1986) J Phys Chem 90:5015
43. Shim I, Gingerich KA (1982) J Chem Phys 76:3833
44. Shim I, Gingerich KA (1984) J Chem Phys 81:5937
45. Balasubramanian K (1990) J Chem Phys 93:8061
46. Balasubramanian K, Liao D (1988) J Chem Phys 88:317
47. Balasubramanian K, Feng PY, Liao MZ (1987) J Chem Phys 87:3981
48. Langhoff SR, Pettersson LGM, Bauschlicher CW, Partridge H (1987) J Chem Phys 86:268
49. Shim I, Gingerich KA (1985) Surf Sci 156:623
50. Russo N, Andzelm J, Salahub DR (1987) Chem Phys 114:331
51. Mayer I (1983) Chem Phys Lett 97:270; (1985) Theoret Chim Acta 67:315; (1986) Int J Quant Chem 29:73, 477
52. Kündig EP, Moskovits M, Ozin GA (1972) Can J Chem 50:3587
53. Pacchioni G, Koutecky J, Fantucci P (1982) Chem Phys Lett 92:486
54. Koutecky J, Pacchioni G, Fantucci P (1985) Chem Phys 99:87
55. Pacchioni G, Koutecky J (1987) J Phys Chem 91:2658
56. Rohlfing CM, Hay PJ (1985) J Chem Phys 83:4641
57. Møller C, Plesset MS (1934) Phys Rev 46:618
58. Blomberg MRA, Lebrilla CB, Siegbahn PEM (1988) Chem Phys Lett 150:522
59. Roos BO, Taylor PR, Siegbahn PEM (1980) Chem Phys 48:157
60. Siegbahn PEM (1983) Int J Quant Chem 23:1869
61. Chong DP, Langhoff SR (1986) J Chem Phys 84:5606
62. Smith GW, Carter EA (1991) J Phys Chem 95:2327
63. Boys SF, Bernardi F (1970) Mol Phys 19:553
64. McKee ML, Worley SD (1988) J Phys Chem 92:3699
65. Mains GJ, White JM (1991) J Phys Chem 95:112
66. Bauschlicher CH, Langhoff SR (1990) Int Rev Phys Chem 9:149
67. Martin RL, Hay PJ (1981) J Chem Phys 75:4539